



CERN-EP-2023-020
17 February 2023

Measurement of the Λ hyperon lifetime

ALICE Collaboration*

Abstract

A new, more precise measurement of the Λ hyperon lifetime is performed using a large data sample of Pb–Pb collisions at $\sqrt{s_{NN}} = 5.02$ TeV with ALICE. The Λ and $\bar{\Lambda}$ hyperons are reconstructed at midrapidity using their two-body weak decay channel $\Lambda \rightarrow p + \pi^-$ and $\bar{\Lambda} \rightarrow \bar{p} + \pi^+$. The measured value of the Λ lifetime is $\tau_{\Lambda} = [261.07 \pm 0.37 \text{ (stat.)} \pm 0.72 \text{ (syst.)}]$ ps. The relative difference between the lifetime of Λ and $\bar{\Lambda}$, which represents an important test of CPT invariance in the strangeness sector, is also measured. The obtained value $(\tau_{\Lambda} - \tau_{\bar{\Lambda}})/\tau_{\Lambda} = 0.0013 \pm 0.0028 \text{ (stat.)} \pm 0.0021 \text{ (syst.)}$ is consistent with zero within the uncertainties. Both measurements of the Λ hyperon lifetime and of the relative difference between τ_{Λ} and $\tau_{\bar{\Lambda}}$ are in agreement with the corresponding world averages of the Particle Data Group and about a factor of three more precise.

arXiv:2303.00606v2 [nucl-ex] 5 Oct 2023

1 Introduction

The Λ is the lightest hyperon, with strangeness $S = -1$, isospin $I = 0$, and quark content uds . Its lifetime has been measured in past experiments starting from 1963 using its weak decay channels $\Lambda \rightarrow p + \pi^-$ and $\bar{\Lambda} \rightarrow \bar{p} + \pi^+$. The world average reported in the Review of Particle Physics of the Particle Data Group (PDG) [1] is $\tau_\Lambda = 263.2 \pm 2.0$ ps. This is the result of averaging the measurements performed in 1973 by Poulard et al. [2] and 1975 by Clayton et al. [3] using Λ produced in interactions of low-energy charged kaon beams with a fixed target, and the measurement of Zech et al. [4] in 1977 using a neutral hyperon beam. These results are based on data samples containing a maximum of fifty-three thousand events. The relative difference between the lifetimes of Λ and $\bar{\Lambda}$ reported in the PDG is $(\tau_\Lambda - \tau_{\bar{\Lambda}})/\tau_\Lambda = -0.001 \pm 0.009$, resulting from the average of two measurements, one performed in 1967 by Badier et al. [5] and another one in 1996 by Barnes et al. [6], using Λ and $\bar{\Lambda}$ produced in low-energy $p + \bar{p} \rightarrow \Lambda + \bar{\Lambda}$ reactions. The excellent tracking and particle-identification capabilities of ALICE over a broad momentum range and the large amount of data collected during Run 2 of the LHC are exploited to improve the current precision on the measurement of the Λ lifetime and on the relative difference between the lifetimes of Λ and $\bar{\Lambda}$. The latter provides a fundamental test of CPT invariance in the strangeness sector.

This measurement is also a fundamental reference for the studies of the properties of hypernuclear states created in heavy-ion collisions and for future precision studies of other hyperon properties. The analysis presented here is performed in Pb–Pb collisions at a center-of-mass energy $\sqrt{s_{NN}} = 5.02$ TeV using the same data sample employed for the measurements of the (anti)hypertriton lifetime and Λ separation energy [7]. The latter measurements are fundamental to infer the internal structure of this hypernucleus as well as the properties of hyperon–nucleon interaction in the low-density limit, as described in [8].

2 Experimental apparatus

ALICE is one of the four large experiments at the LHC and it is dedicated to the study of heavy-ion collisions at ultrarelativistic energies. A detailed description of the ALICE apparatus and its performance can be found in Refs. [9] and [10]. In the following, only the subdetector systems used for the analysis presented in this paper are described.

Trajectories of charged particles are reconstructed in the ALICE central barrel with the Inner Tracking System (ITS) [11] and the Time Projection Chamber (TPC) [12]. These are located within a large solenoidal magnet, providing a highly homogeneous magnetic field of 0.5 T parallel to the beam axis. The ITS consists of six cylindrical layers of silicon detectors, concentric and coaxial to the beam pipe, with a total pseudorapidity coverage $|\eta| < 0.9$ with respect to the nominal interaction point. Three different technologies are used for this detector: the two innermost layers consist of silicon pixel detectors (SPD), the two central layers of silicon drift detectors (SDD), and the two outermost layers of double-sided silicon strip detectors (SSD). This detector is used in the determination of primary and secondary vertices, and in the track reconstruction.

The TPC is the largest detector in the ALICE central barrel, with a pseudorapidity coverage $|\eta| < 0.9$. It is used for charged-particle track reconstruction, momentum measurement, and particle identification (PID) via the measurement of the specific energy loss (dE/dx) of particles in the TPC gas. This detector provides up to 159 spacial points per track for charged-particle reconstruction. The resolution in the measurement of the distance-of-closest approach of primary tracks to the primary collision vertex, projected on the transverse plane, ranges from about 200 μm at 0.2 GeV/ c to about 10 μm at 10 GeV/ c [10]. The transverse-momentum (p_T) resolution ranges from about 1% at 1 GeV/ c to about 10% at 50 GeV/ c in Pb–Pb collisions at $\sqrt{s_{NN}} = 5.02$ TeV [13]. The dE/dx resolution depends on the event multiplicity and is about 5–6.5% for minimum-ionizing particles crossing the full volume of the TPC [10].

The PID is complemented by the Time-Of-Flight (TOF) system [14]. This detector is made of Multi-

gap Resistive Plate Chambers (MRPC) and is located at a radial distance of 3.7 m from the nominal interaction point. The TOF detector measures the arrival time of particles relative to the event collision time provided by the TOF detector itself or by the T0 detectors, two arrays of Cherenkov counters located at forward and backward rapidities [15]. The TOF detector is used in this analysis for pile-up rejection, mostly from out-of-bunch collisions, by requiring that at least one of the Λ ($\bar{\Lambda}$) charged decay-daughter tracks has an associated hit in the TOF detector.

Collision events are triggered by two plastic scintillator arrays, V0A and V0C [16], located on both sides of the interaction point, covering the pseudorapidity regions $2.8 < \eta < 5.1$ and $-3.7 < \eta < -1.7$, respectively. Each array consists of four concentric rings, each ring comprising eight cells with the same azimuthal coverage. The V0A and V0C scintillators are used to determine the collision centrality from the measured signals produced by charged particles [17, 18]. The centrality is defined in terms of percentiles of the total hadronic cross section.

3 Data analysis

3.1 Event selection

The data used for this analysis were collected in 2018 during the LHC Pb–Pb run at $\sqrt{s_{\text{NN}}} = 5.02$ TeV. A minimum bias (MB) event trigger and two centrality triggers were used. The MB trigger, fully efficient in the centrality interval 0–90%, requires coincident signals in the V0 detectors, synchronous with the bunch crossing time defined by the LHC clock. The two centrality triggers, fully efficient in the centrality classes 0–10% and 30–50%, are based on the signal amplitude measured by the V0 scintillators, which is proportional to the charged-particle multiplicity of the event. The analysis is performed in four centrality classes: 0–10%, 10–30%, 30–50%, and 50–90%. The events in the centrality classes 0–10% and 30–50% are selected using both the MB and centrality triggers, while the MB event trigger alone is used for the other centrality classes. In order to keep the conditions of the detectors as uniform as possible and reject background collisions, the coordinate of the primary vertex along the beam axis is required to be within 10 cm from the nominal interaction point. Events with multiple vertices identified with the SPD are tagged as pile-up and removed from the analysis [10]. In addition, events with pile-up occurring during the drift time of the TPC are rejected based on the correlation between the number of SDD and SSD clusters and the total number of clusters in the TPC, as described in Ref. [19]. To further suppress the pile-up contribution, mostly from out-of-bunch collisions, the Λ daughter tracks are required to have an associated hit in the TOF detector. This requirement is applied only for the centrality classes 30–50% and 50–90%. For the most central events, the matching of daughter tracks with a TOF hit does not have a significant impact on the fraction of Λ ($\bar{\Lambda}$) from events with out-of-bunch pile-up, which is found to be between 0.02% and 0.07%. The total number of events selected for each centrality class is reported in Table 1.

Table 1: Number of events used for the analysis.

Centrality	Number of events ($\times 10^6$)
0–10%	70.97
10–30%	18.43
30–50%	61.43
50–90%	36.86

3.2 Selection of Λ candidates

The two-body decay channels $\Lambda \rightarrow p + \pi^-$ and $\bar{\Lambda} \rightarrow \bar{p} + \pi^+$ are used in this measurement. These have a branching ratio BR of $(63.9 \pm 0.5)\%$ [1]. The Λ ($\bar{\Lambda}$) candidates are reconstructed using the standard AL-

ICE weak decay finder. This algorithm searches for weak decay topologies, called V^0 , by reconstructing oppositely-charged particle tracks originating from a displaced vertex as described in Refs. [20, 21]. In the case of a decay vertex located inside the ITS volume, at least one hit in any of the ITS layers is used in the reconstruction of the charged tracks originating from the V^0 decay. The reconstructed tracks, selected in the pseudorapidity region $|\eta| < 0.8$, are required to fulfil a set of quality criteria such as having a number of TPC crossed rows larger than 80, a number of TPC clusters used for the dE/dx calculation larger than 60 to ensure a good dE/dx resolution, a fraction of TPC crossed rows and findable clusters larger than 70%, and a good track fit $\chi^2/N_{\text{cls}}^{\text{TPC}} < 2.5$, where $N_{\text{cls}}^{\text{TPC}}$ is the number of TPC clusters.

To reduce the combinatorial background, a set of topological selections are applied, i.e. the distance of closest approach (DCA) between the V^0 daughter tracks is required to be less than 1 cm, the DCA between the V^0 and the primary collision vertex less than 0.5 cm, the radial distance between primary and secondary vertices larger than 3 cm, and $\cos(\theta_p) > 0.995$, where θ_p is the angle between the vector connecting the primary and secondary vertices and the total V^0 momentum ($\vec{p}_{V^0} = \vec{p}_p + \vec{p}_\pi$). The selection criteria applied for this measurement are similar to those already used in previous measurements [21–23].

The particle identification is based on the energy loss per unit of track length measured by the TPC. Protons and pions are identified by requiring that their measured dE/dx is within $3\sigma_{dE/dx}$ from the expected average calculated using the Bethe–Bloch, where $\sigma_{dE/dx}$ is the dE/dx resolution. Proton and pion candidates are selected in the transverse-momentum intervals $0.2 < p_T^\pi < 2 \text{ GeV}/c$ and $0.2 < p_T^p < 10 \text{ GeV}/c$, respectively.

3.3 Signal extraction

The Λ and $\bar{\Lambda}$ lifetimes are extracted from a fit to their proper decay length distributions using the exponential function $\exp(-L_{\text{proper}}/\langle L_{\text{proper}} \rangle)$. The proper decay length is calculated for every Λ ($\bar{\Lambda}$) as

$$L_{\text{proper}} = L_{\text{lab}}/\beta\gamma = M_\Lambda \frac{L_{\text{lab}}}{p}, \quad (1)$$

where L_{lab} is the decay length measured in the laboratory system as the distance between primary and secondary vertices, M_Λ is the Λ mass taken from the PDG ($M_\Lambda = 1115.683 \text{ MeV}/c^2$) [1], and p is the total momentum of the Λ ($\bar{\Lambda}$) measured at the decay point. The number of signal counts in each L_{proper} interval is obtained using the following procedure, which is illustrated in Fig. 1:

1. **Location of the peak region:** the invariant mass of the decay daughters is calculated and the region around the maximum of the invariant-mass distribution is fitted using a Gaussian function. The peak region is defined as $[M_0 - 8\sigma, M_0 + 10\sigma]$, where M_0 is the mean and σ is the standard deviation of the Gaussian fit. The choice of such a wide signal region is motivated by the fact that the peak has two long tails and is slightly asymmetric, especially for low values of L_{proper} . This asymmetry is an effect of residual imperfections in tracking and energy loss corrections, which affect candidates with invariant masses above and below the expected mass differently.
2. **Fit of the background:** the background on the side bands of the peak is fitted using a continuous function to extrapolate the expected background inside the peak region. Since the background shape changes with L_{proper} , a third-order polynomial function is used to fit the background at low L_{proper} while the sum of a power-law and a linear function is used at high L_{proper} values. These functions have the minimum number of parameters that guarantees a data-to-fit ratio consistent with unity within statistical uncertainties in the sidebands.
3. **Signal extraction:** the signal is extracted in each L_{proper} interval by subtracting the estimated background from the invariant mass distribution and counting the entries inside the peak region.

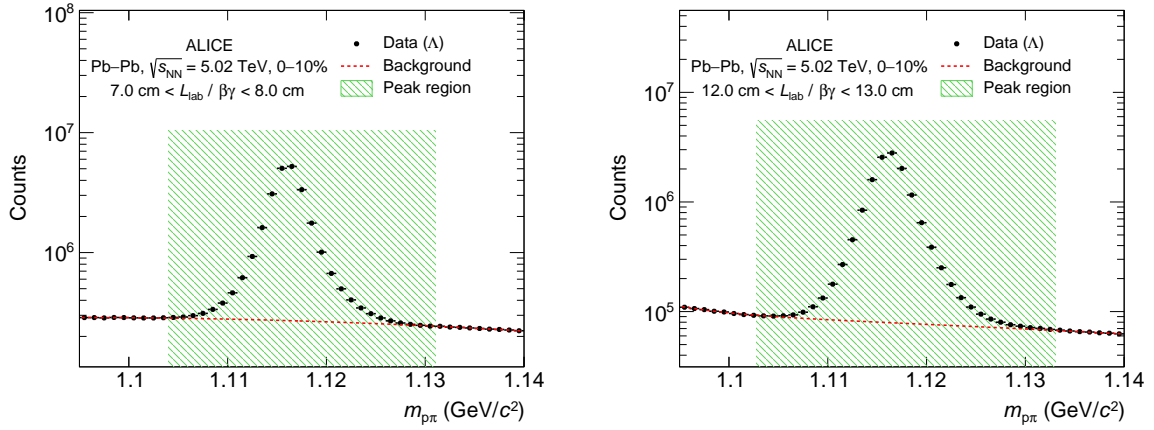


Figure 1: Invariant mass spectra of $p\pi$ pairs measured in central collisions (0–10%) at low (left) and large (right) L_{proper} . The green area indicates the peak region.

The total number of Λ and $\bar{\Lambda}$ raw counts within the peak region are reported in Table 2 for each centrality interval.

Table 2: Raw counts of Λ and $\bar{\Lambda}$ for different centralities.

Centrality	$\Lambda (\times 10^6)$	$\bar{\Lambda} (\times 10^6)$
0–10%	312.6	296.4
10–30%	49.7	47.2
30–50%	41.2	35.9
50–90%	4.2	3.6

3.4 Efficiency and secondary Λ corrections

The raw L_{proper} spectrum of Λ ($\bar{\Lambda}$) is corrected for the reconstruction efficiency, the feed-down contribution from higher-mass baryons and secondary Λ ($\bar{\Lambda}$) originating from interactions of particles with the detector material as

$$\left[\frac{dN_{\Lambda}}{dL_{\text{proper}}} \right]_{\text{corr}} = \frac{1}{\varepsilon(L_{\text{proper}})} \times f_{\text{prim}}(L_{\text{proper}}) \times \left[\frac{dN_{\Lambda}}{dL_{\text{proper}}} \right]_{\text{raw}}, \quad (2)$$

where $\varepsilon(L_{\text{proper}})$ is the efficiency of primary Λ ($\bar{\Lambda}$) and $f_{\text{prim}}(L_{\text{proper}})$ is the fraction of primary Λ ($\bar{\Lambda}$). The dominant feed-down contributions are given by the weak decays of Ξ^{\pm} , Ξ^0 , and Ω^{\pm} : [1]

- $\Xi^0(\bar{\Xi}^0) \rightarrow \Lambda(\bar{\Lambda}) + \pi^0$ BR = $(99.524 \pm 0.012)\%$,
- $\Xi^{\pm} \rightarrow \Lambda + \pi^{\pm}$ BR = $(99.887 \pm 0.035)\%$,
- $\Omega^{\pm} \rightarrow \Lambda + K^{\pm}$ BR = $(67.8 \pm 0.7)\%$,
- $\Omega^{\pm} \rightarrow \Xi^0 + \pi^{\pm}$ and $\Omega^{\pm} \rightarrow \Xi^{\pm} + \pi^0$ BR = $(32.2 \pm 0.8)\%$.

These corrections are calculated using Monte Carlo (MC) simulations. Collision events between lead ions are simulated using the HIJING event generator [24] and the passage of particles through the experimental apparatus is simulated using GEANT3 [25] as transport code. Considering that the p_T distributions of particles and their relative abundances in MC simulations are different from data, centrality and

p_T -dependent corrections are applied in MC simulations using weights. These are defined, for different centrality classes, as the ratio of the p_T spectrum measured by ALICE and the p_T spectrum generated by HIJING.

The ALICE measurements of the p_T spectra of Λ , Ξ^\pm , and Ω^\pm [21, 26] in Pb–Pb collisions at $\sqrt{s_{NN}} = 2.76$ TeV, scaled by the ratio of the proton p_T spectra measured at $\sqrt{s_{NN}} = 5.02$ TeV [27] and $\sqrt{s_{NN}} = 2.76$ TeV [28], are used to calculate the weights for different centralities. Based on isospin symmetry, the p_T spectra of Ξ^0 are assumed to be identical to those of Ξ^\pm . Centrality dependent factors, given by the ratios $(\Xi/\Lambda)_{\text{data}}/(\Xi/\Lambda)_{\text{MC}}$ and $(\Omega/\Lambda)_{\text{data}}/(\Omega/\Lambda)_{\text{MC}}$, are also included to reproduce the centrality dependence of the particle ratios observed in data. The efficiency is calculated as the ratio between reconstructed and generated primary Λ in the simulation

$$\varepsilon(L_{\text{proper}}) = \frac{\left[\frac{dN_\Lambda}{dL_{\text{proper}}} \right]_{\text{rec}}}{\left[\frac{dN_\Lambda}{dL_{\text{proper}}} \right]_{\text{gen}}}. \quad (3)$$

The efficiencies of Λ and $\bar{\Lambda}$ for central Pb–Pb collisions (0–10%) as a function of L_{proper} are shown in Fig. 2 (left). The correction for secondary Λ ($\bar{\Lambda}$) from material and weak decays is applied by scaling the raw L_{proper} spectrum by the fraction of primary Λ ($\bar{\Lambda}$) given by

$$f_{\text{prim}}(L_{\text{proper}}) = 1 - \frac{dN_{\Lambda_{\text{sec}}}/dL_{\text{proper}}}{dN_{\Lambda_{\text{all}}}/dL_{\text{proper}}}. \quad (4)$$

The fraction of secondary Λ and $\bar{\Lambda}$ for central Pb–Pb (0–10%) is shown as a function of L_{proper} in the right panel of Fig. 2. The individual contributions from material and weak decays are shown in addition to the total fraction for illustration. The observed trend of the fraction of secondary Λ ($\bar{\Lambda}$) from weak decays with L_{proper} is due to an interplay between the efficiency and decay time of the Λ ($\bar{\Lambda}$) mother particle. For secondary Λ ($\bar{\Lambda}$) from material, it is due to a combined effect of efficiency and the radial distance at which the secondary Λ ($\bar{\Lambda}$) is produced.

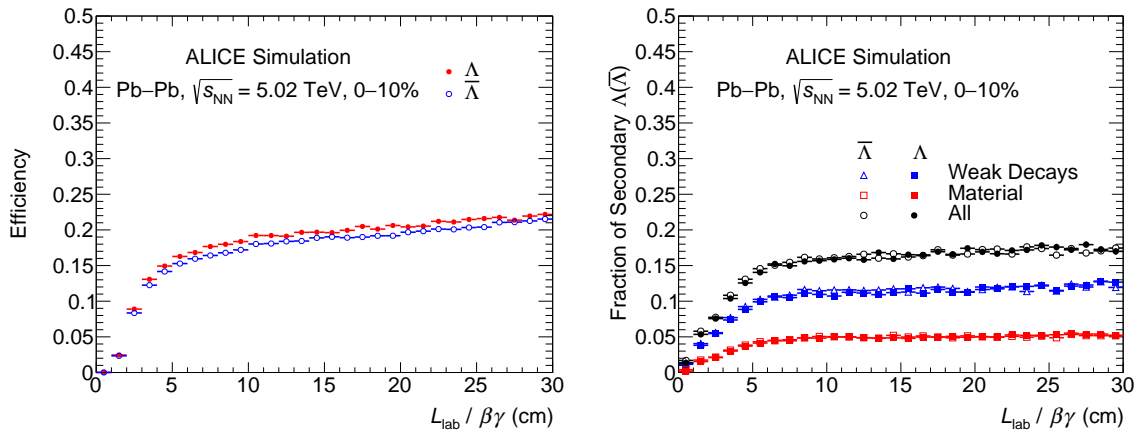


Figure 2: Reconstruction efficiency of primary Λ ($\bar{\Lambda}$) (left) and fraction of secondary Λ ($\bar{\Lambda}$) (right) in central Pb–Pb collisions (0–10%).

4 Systematic uncertainties

The dominant sources of systematic uncertainties on the Λ and $\bar{\Lambda}$ lifetime measurements are related to the track and V^0 selections, signal extraction, efficiency and feed-down corrections. These are summarized

in Table 3. The methods used to estimate the systematic uncertainties from these sources are illustrated in the following. In addition, effects of the material budget uncertainty, the uncertainty on the hadronic interaction of Λ , $\bar{\Lambda}$, and their decay daughters, and potential effects of residual pile-up—which are found to be negligible—are also discussed.

Table 3: Summary of the systematic uncertainties on the Λ and $\bar{\Lambda}$ lifetime measurements. All values are in ps.

Source	Λ	$\bar{\Lambda}$	$\Lambda + \bar{\Lambda}$
Track and V^0 selections	0.55	0.69	0.65
Signal extraction	0.03	0.03	0.02
Efficiency and feed-down corrections	0.30	0.33	0.30
Total	0.63	0.77	0.72

4.1 Systematic uncertainty from track and V^0 selection

The systematic uncertainty due to the track and V^0 selection criteria is estimated by repeating the full analysis chain using one hundred different analysis parameters, where the single-track, topological, and particle-identification selection criteria are varied, such that they produce a maximum variation of $\pm 10\%$ in the raw signal yield, similarly to the approach used in Refs. [21–23]. The systematic uncertainty from the track and V^0 selection is calculated by fitting the distribution of lifetime values obtained from different selection criteria using a Gaussian function and taking the σ of the Gaussian fit as an uncertainty. The obtained uncertainties are 0.55 ps for τ_Λ , 0.69 ps for $\tau_{\bar{\Lambda}}$, and 0.65 ps for $\tau_{\Lambda+\bar{\Lambda}}$. This contribution is the dominant source of systematic uncertainty.

4.2 Signal extraction uncertainty

The systematic uncertainty from the signal extraction includes two contributions: the choice of the background fit range and the integration range used for the raw yield extraction. For both contributions, one hundred different intervals are randomly generated, with a uniform probability distribution between two extremes, and the signal extraction procedure is repeated for each of these intervals. The limits used are specified in Table 4.

Table 4: Invariant-mass intervals used for the signal extraction systematic uncertainty.

	Left extreme	Right extreme
Background fit range	$[M_0 - 14\sigma, M_0 - 11\sigma]$	$[M_0 + 20\sigma, M_0 + 32\sigma]$
Signal integration range	$[M_0 - 13\sigma, M_0 - 7\sigma]$	$[M_0 + 5\sigma, M_0 + 11\sigma]$

The standard deviation of the distribution of raw yields in each L_{proper} interval is taken as the systematic uncertainty. These two contributions are independent and added in quadrature. The stability of the results was tested against different choices of the fit functions used to model the background. In particular, linear and second-order polynomials were also tried at low L_{proper} , while an exponential (power-law) for the left and second-order polynomial (exponential) for the right side of the background were also used at high L_{proper} . The use of alternative fit functions to model the background resulted in negligible changes in the extracted yield. For this reason, this contribution to the signal extraction uncertainty is considered negligible. The uncertainty on the lifetime is calculated by replacing the statistical uncertainties on the corrected L_{proper} spectrum with the signal extraction uncertainties, which are bin-by-bin uncorrelated, and taking the uncertainty from the exponential fit as the systematic uncertainty. This contribution is found to be $(\Delta\tau)_{\text{signal}}^{\text{syst}} = 0.03$ ps for both τ_Λ and $\tau_{\bar{\Lambda}}$, and 0.02 ps for $\tau_{\Lambda+\bar{\Lambda}}$.

4.3 Systematic uncertainty from efficiency and feed-down corrections

The systematic uncertainty related to the efficiency and feed-down corrections is estimated by varying: (i) the p_T -dependent weights used to adjust the input p_T distributions of Λ , Ξ , and Ω in the simulations, (ii) the Λ , Ξ , and Ω lifetimes by the PDG uncertainties [1] and (iii) the Λ/Ξ and Λ/Ω ratios by the measured uncertainties. The Ω is found to give a negligible contribution to the systematic uncertainties. To vary the lifetimes implemented in the simulations, which are taken from the PDG [1], L_{proper} -dependent weights are used. These are obtained as the ratio between the L_{proper} spectrum with modified lifetime and the default spectrum. To estimate the total contribution of these sources, a set of five hundred different efficiency and feed-down corrections is generated. Each of them is obtained using a different set of weights where the p_T spectra of Λ , Ξ , and Ω , their lifetimes and particle ratios are varied by a fraction of their uncertainty. Such a fraction is extracted randomly from a Gaussian distribution centered at zero and with a width equal to 1. When modifying the p_T spectra measured in data to recalculate the weights, the correlated and uncorrelated uncertainties with p_T are treated differently:

1. **p_T -correlated uncertainties:** all data points of the p_T spectrum are shifted coherently upward and downward by a fraction of their systematic uncertainty in each p_T interval.
2. **p_T -uncorrelated uncertainties:** the data points are moved independently by a fraction of their uncorrelated uncertainty in each p_T interval.

These five hundred different efficiencies and fractions of secondary Λ ($\bar{\Lambda}$) are then used to correct the raw- L_{proper} spectrum measured in data. The lifetime is extracted for each corrected spectrum and the standard deviation of the distribution of lifetimes is taken as an estimate of the systematic uncertainty from efficiency and feed-down corrections. The obtained uncertainties are 0.30 ps for τ_Λ , 0.33 ps for $\tau_{\bar{\Lambda}}$, and 0.30 ps for $\tau_{\Lambda+\bar{\Lambda}}$.

4.4 Inelastic interaction with the detector materials

The default efficiency is based on GEANT3 transport package. The effect of (anti)matter absorption was studied by comparing the default efficiency with that obtained using a MC production based on GEANT4 [29], which contains slightly different parametrizations of the inelastic cross sections of (anti)matter particles. The GEANT3 and GEANT4-based efficiencies are consistent within uncertainties. The Λ and $\bar{\Lambda}$ lifetimes are found to be consistent within uncertainties, and therefore, no systematic uncertainty is assigned due to this effect.

4.5 Material budget

The ALICE detector material is known with a precision of 4.5% [10]. The effect of the limited knowledge of the material budget, which could affect the efficiency and the fraction of secondary Λ ($\bar{\Lambda}$) from material and its dependence on L_{proper} , is studied by comparing the efficiency and corrections for secondary Λ ($\bar{\Lambda}$) using MC productions with increased and decreased material density by 4.5%. The difference in the mean lifetime is found to not be statistically significant and therefore this contribution is neglected.

4.6 Pile-up effects

Simultaneous collisions with displaced vertices (pile-up) could, in principle, create a bias in the measurement of the Λ ($\bar{\Lambda}$) decay length due to the wrong V^0 -vertex association. The tight selection on the $\cos(\theta_p)$ allows the matching between a reconstructed V^0 and the wrong vertex only for close vertices. This happens with very low probability and is found to give a negligible bias in the decay length measurement. To further cross-check potential pile-up effects, the analysis is repeated removing all pile-up

rejections. The Λ ($\bar{\Lambda}$) lifetimes, in this case, are found to be consistent with the value using default pile-up rejection within the statistical uncertainties. It is concluded that the pile-up effects combined with rather strong topological selections used in this analysis give a negligible effect on the Λ ($\bar{\Lambda}$) lifetime.

5 Results

The L_{proper} spectra of Λ and $\bar{\Lambda}$ measured in each centrality interval are corrected for the corresponding efficiency, feed-down from higher mass baryons, and the fraction of secondary Λ ($\bar{\Lambda}$) from the material. The use of centrality triggers in the data used in this analysis leads to a non-uniform centrality distribution. In order to restore the correct relative contribution from different centralities, the L_{proper} spectra measured in the centrality intervals 10–30%, 30–50%, and 50–90% are scaled by a factor

$$k_i = \frac{N_{\text{events}}^{0-10\%} / w_{0-10\%}}{N_{\text{events}}^i / w_i} w_i, \quad (5)$$

where N_{events}^i and w_i are the number of events and the centrality bin width of the i -th centrality interval and $N_{\text{events}}^{0-10\%}$ and $w_{0-10\%} = 10$ are those related to the reference centrality interval 0–10%. The obtained spectrum is normalized to unity and fitted with an exponential function in the L_{proper} interval [3,30] cm to extract the mean lifetime. The fit results for Λ , $\bar{\Lambda}$ and their sum are shown in Fig. 3, which also contains the data-to-fit ratios in the bottom panels. The data-to-fit ratio in each interval is obtained as the ratio between the interval content and the weighted average of the fit function within the interval, with weight given by the exponential function. In this figure, only statistical uncertainties in each L_{proper} interval and on the mean lifetime are shown. The systematic uncertainties are calculated using the procedure described in Sec. 4 and are reported only for the final result of the lifetime in the 0–90% centrality class. The fit is stable when changing fit range ($L_{\text{proper}}^{\text{min}} = 1, 2, 3, 4, 5, \dots, 10$ cm) and binning (width = 0.5, 1, 2 cm) leading to results that are consistent within the statistical uncertainties.

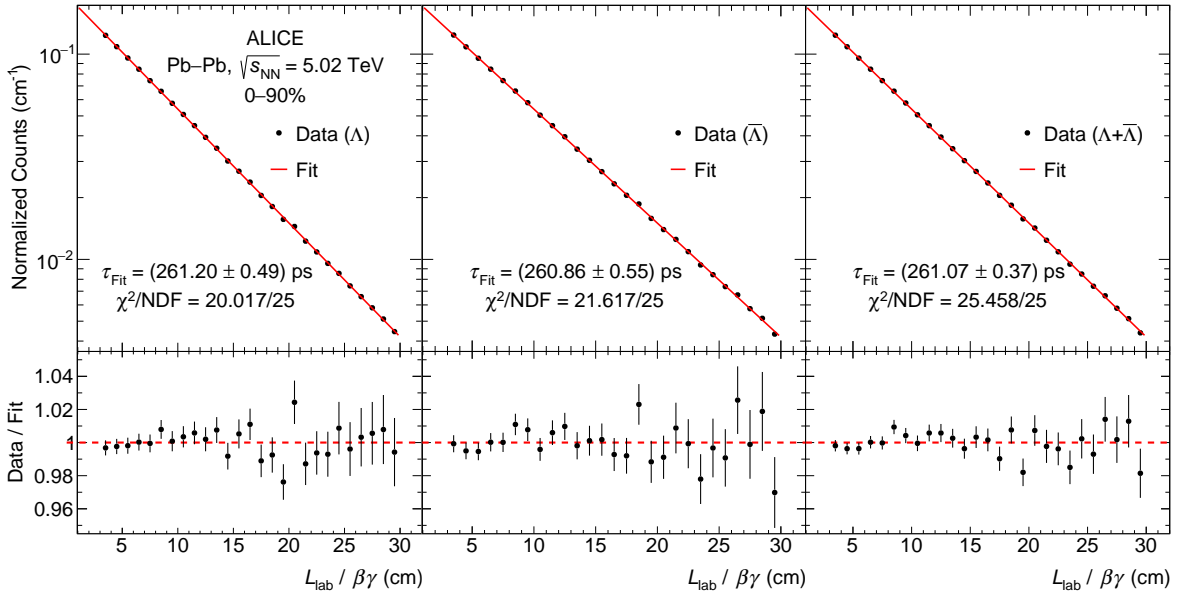


Figure 3: L_{proper} spectra of Λ (left), $\bar{\Lambda}$ (middle) and their sum (right), and exponential fits for the lifetime extractions. Only statistical uncertainties are shown for each data point and for the mean lifetime extracted from the exponential fit.

The measured lifetimes of Λ and $\bar{\Lambda}$ with statistical and systematic uncertainties, are

$$\begin{aligned}\tau_{\Lambda} &= [261.20 \pm 0.49(\text{stat.}) \pm 0.63(\text{syst.})] \text{ ps}, \\ \tau_{\bar{\Lambda}} &= [260.86 \pm 0.55(\text{stat.}) \pm 0.77(\text{syst.})] \text{ ps}, \\ \tau_{\Lambda+\bar{\Lambda}} &= [261.07 \pm 0.37(\text{stat.}) \pm 0.72(\text{syst.})] \text{ ps}.\end{aligned}$$

The lifetimes extracted in different centrality intervals are consistent within their statistical uncertainties, as shown in Fig. 4. As a cross-check, the lifetime is also calculated as the weighted average of the results in different centrality intervals, with weights given by the inverse of the statistical uncertainties squared. The result is fully consistent with that extracted from the L_{proper} distribution obtained using Eq. 5.

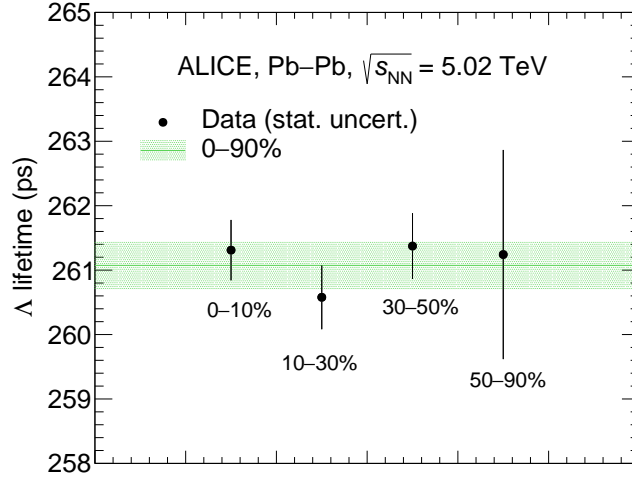


Figure 4: Λ lifetime measured in different centrality intervals. Only statistical uncertainties are shown.

The present measurement is compared with previous results in Fig. 5. The STAR measurement is taken from Ref. [30]. For this comparison, statistical and systematic uncertainties are added in quadrature.

Assuming CPT invariance, the lifetimes of the Λ and $\bar{\Lambda}$ are expected to be consistent within uncertainties. To test CPT invariance, the relative difference $(\tau_{\Lambda} - \tau_{\bar{\Lambda}})/\tau_{\Lambda}$ is measured. Statistical uncertainties on τ_{Λ} and $\tau_{\bar{\Lambda}}$ and the systematic uncertainties originating from the signal extraction are uncorrelated and propagated independently. On the other hand, the systematic uncertainties on the efficiency and feed-down corrections as well as those on the track and V^0 selections of Λ and $\bar{\Lambda}$ are partially correlated. The systematic uncertainty on the relative difference $(\tau_{\Lambda} - \tau_{\bar{\Lambda}})/\tau_{\Lambda}$ from the former contribution is considered as half of the interval with the following extremes

$$\left[\frac{\tau_{\bar{\Lambda}}}{\tau_{\Lambda}} \right]_{\text{upper}} = \frac{\tau_{\bar{\Lambda}} + \Delta\tau_{\bar{\Lambda}}(\text{corrections})}{\tau_{\Lambda} + \Delta\tau_{\Lambda}(\text{corrections})}, \quad (6)$$

$$\left[\frac{\tau_{\bar{\Lambda}}}{\tau_{\Lambda}} \right]_{\text{lower}} = \frac{\tau_{\bar{\Lambda}} - \Delta\tau_{\bar{\Lambda}}(\text{corrections})}{\tau_{\Lambda} - \Delta\tau_{\Lambda}(\text{corrections})}, \quad (7)$$

and is found to be 1.1×10^{-4} . To take into account the correlation between the uncertainties from the track and V^0 selections, the relative difference $(\tau_{\Lambda} - \tau_{\bar{\Lambda}})/\tau_{\Lambda}$ is calculated for each of the different analysis settings used. The uncertainty is given by the standard deviation of the distribution of $(\tau_{\Lambda} - \tau_{\bar{\Lambda}})/\tau_{\Lambda}$

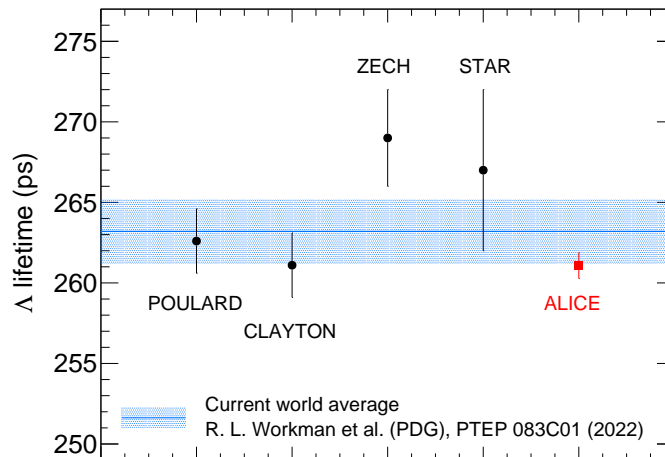


Figure 5: ALICE measurement of the Λ lifetime in comparison with previous measurements [2–4, 30] and the current world average taken from the PDG [1]. Statistical and systematic uncertainties are added in quadrature.

values and is found to be 0.0021, which is the largest contribution to the total systematic uncertainty. The measured value of the relative difference between the Λ and $\bar{\Lambda}$ lifetimes is

$$(\tau_{\Lambda} - \tau_{\bar{\Lambda}})/\tau_{\Lambda} = 0.0013 \pm 0.0028(\text{stat.}) \pm 0.0021(\text{syst.}), \quad (8)$$

while that reported in the PDG is $(\tau_{\Lambda} - \tau_{\bar{\Lambda}})/\tau_{\Lambda} = -0.001 \pm 0.009$ [1]. The present measurement is consistent with zero with an overall improvement of the absolute precision with respect to the PDG by approximately a factor of three.

6 Summary

Unprecedentedly precise measurements of the Λ ($\bar{\Lambda}$) lifetime and of the relative difference between the lifetimes of Λ and $\bar{\Lambda}$ are presented. The latter represents an important test of the CPT symmetry in the strangeness sector. The confidence range of the Λ ($\bar{\Lambda}$) lifetime is reduced by approximately a factor of three with respect to the PDG average.

Acknowledgements

The ALICE Collaboration would like to thank all its engineers and technicians for their invaluable contributions to the construction of the experiment and the CERN accelerator teams for the outstanding performance of the LHC complex. The ALICE Collaboration gratefully acknowledges the resources and support provided by all Grid centres and the Worldwide LHC Computing Grid (WLCG) collaboration. The ALICE Collaboration acknowledges the following funding agencies for their support in building and running the ALICE detector: A. I. Alikhanyan National Science Laboratory (Yerevan Physics Institute) Foundation (ANSL), State Committee of Science and World Federation of Scientists (WFS), Armenia; Austrian Academy of Sciences, Austrian Science Fund (FWF): [M 2467-N36] and Nationalstiftung für Forschung, Technologie und Entwicklung, Austria; Ministry of Communications and High Technologies, National Nuclear Research Center, Azerbaijan; Conselho Nacional de Desenvolvimento Científico e Tecnológico (CNPq), Financiadora de Estudos e Projetos (Finep), Fundação de Amparo à Pesquisa do Estado de São Paulo (FAPESP) and Universidade Federal do Rio Grande do Sul (UFRGS),

Brazil; Bulgarian Ministry of Education and Science, within the National Roadmap for Research Infrastructures 2020-2027 (object CERN), Bulgaria; Ministry of Education of China (MOEC), Ministry of Science & Technology of China (MSTC) and National Natural Science Foundation of China (NSFC), China; Ministry of Science and Education and Croatian Science Foundation, Croatia; Centro de Aplicaciones Tecnológicas y Desarrollo Nuclear (CEADEN), Cubaenergía, Cuba; Ministry of Education, Youth and Sports of the Czech Republic, Czech Republic; The Danish Council for Independent Research | Natural Sciences, the VILLUM FONDEN and Danish National Research Foundation (DNRF), Denmark; Helsinki Institute of Physics (HIP), Finland; Commissariat à l’Energie Atomique (CEA) and Institut National de Physique Nucléaire et de Physique des Particules (IN2P3) and Centre National de la Recherche Scientifique (CNRS), France; Bundesministerium für Bildung und Forschung (BMBF) and GSI Helmholtzzentrum für Schwerionenforschung GmbH, Germany; General Secretariat for Research and Technology, Ministry of Education, Research and Religions, Greece; National Research, Development and Innovation Office, Hungary; Department of Atomic Energy Government of India (DAE), Department of Science and Technology, Government of India (DST), University Grants Commission, Government of India (UGC) and Council of Scientific and Industrial Research (CSIR), India; National Research and Innovation Agency - BRIN, Indonesia; Istituto Nazionale di Fisica Nucleare (INFN), Italy; Japanese Ministry of Education, Culture, Sports, Science and Technology (MEXT) and Japan Society for the Promotion of Science (JSPS) KAKENHI, Japan; Consejo Nacional de Ciencia (CONACYT) y Tecnología, through Fondo de Cooperación Internacional en Ciencia y Tecnología (FONCICYT) and Dirección General de Asuntos del Personal Académico (DGAPA), Mexico; Nederlandse Organisatie voor Wetenschappelijk Onderzoek (NWO), Netherlands; The Research Council of Norway, Norway; Commission on Science and Technology for Sustainable Development in the South (COMSATS), Pakistan; Pontificia Universidad Católica del Perú, Peru; Ministry of Education and Science, National Science Centre and WUT ID-UB, Poland; Korea Institute of Science and Technology Information and National Research Foundation of Korea (NRF), Republic of Korea; Ministry of Education and Scientific Research, Institute of Atomic Physics, Ministry of Research and Innovation and Institute of Atomic Physics and University Politehnica of Bucharest, Romania; Ministry of Education, Science, Research and Sport of the Slovak Republic, Slovakia; National Research Foundation of South Africa, South Africa; Swedish Research Council (VR) and Knut & Alice Wallenberg Foundation (KAW), Sweden; European Organization for Nuclear Research, Switzerland; Suranaree University of Technology (SUT), National Science and Technology Development Agency (NSTDA), Thailand Science Research and Innovation (TSRI) and National Science, Research and Innovation Fund (NSRF), Thailand; Turkish Energy, Nuclear and Mineral Research Agency (TENMAK), Turkey; National Academy of Sciences of Ukraine, Ukraine; Science and Technology Facilities Council (STFC), United Kingdom; National Science Foundation of the United States of America (NSF) and United States Department of Energy, Office of Nuclear Physics (DOE NP), United States of America. In addition, individual groups or members have received support from: European Research Council, Strong 2020 - Horizon 2020, Marie Skłodowska Curie (grant nos. 950692, 824093, 896850), European Union; Academy of Finland (Center of Excellence in Quark Matter) (grant nos. 346327, 346328), Finland; Programa de Apoyos para la Superación del Personal Académico, UNAM, Mexico;

References












- [1] **Particle Data Group** Collaboration, R. L. Workman *et al.*, “Review of Particle Physics”, *Prog. Theor. Exp. Phys.* **2022** (2022) 083C01.
- [2] G. Poulard, A. Givernaud, and A. Borg, “New measurement of the Λ lifetime”, *Phys. Lett. B* **46** (1973) 135–137.
- [3] E. F. Clayton *et al.*, “High-statistics determination of the Λ mean lifetime”, *Nucl. Phys. B* **95** (1975) 130–134.

- [4] G. Zech *et al.*, “A Measurement of the Lifetimes of Ξ^0 and Λ Hyperons”, *Nucl. Phys. B* **124** (1977) 413–425.
- [5] J. Badier *et al.*, “Reactions $pp \rightarrow \Lambda\Lambda$ at 2.5 GeV/c”, *Phys. Lett. B* **25** (1967) 152–155.
- [6] P. D. Barnes *et al.*, “Observables in high statistics measurements of the reaction $\bar{p}p \rightarrow \bar{\Lambda}\Lambda$ ”, *Phys. Rev. C* **54** (Oct, 1996) 1877–1886.
- [7] ALICE Collaboration, S. Acharya *et al.*, “Measurement of the lifetime and Λ separation energy of ${}^3\Lambda\text{H}$ ”, *Phys. Rev. Lett.* **131** (2023) 102302, arXiv:2209.07360 [nucl-ex].
- [8] ALICE Collaboration, “The ALICE experiment – A journey through QCD”, arXiv:2211.04384 [nucl-ex].
- [9] ALICE Collaboration, K. Aamodt *et al.*, “The ALICE experiment at the CERN LHC”, *JINST* **3** (2008) S08002.
- [10] ALICE Collaboration, B. Abelev *et al.*, “Performance of the ALICE Experiment at the CERN LHC”, *Int. J. Mod. Phys. A* **29** (2014) 1430044, arXiv:1402.4476 [nucl-ex].
- [11] ALICE Collaboration, K. Aamodt *et al.*, “Alignment of the ALICE Inner Tracking System with cosmic-ray tracks”, *JINST* **5** (2010) P03003, arXiv:1001.0502 [physics.ins-det].
- [12] J. Alme *et al.*, “The ALICE TPC, a large 3-dimensional tracking device with fast readout for ultra-high multiplicity events”, *Nucl. Instrum. Meth. A* **622** (2010) 316–367, arXiv:1001.1950 [physics.ins-det].
- [13] ALICE Collaboration, S. Acharya *et al.*, “Transverse momentum spectra and nuclear modification factors of charged particles in pp, p – Pb and Pb – Pb collisions at the LHC”, *JHEP* **11** (2018) 013, arXiv:1802.09145 [nucl-ex].
- [14] A. Akindinov *et al.*, “Performance of the ALICE Time-Of-Flight detector at the LHC”, *Eur. Phys. J. Plus* **128** (2013) 44.
- [15] ALICE Collaboration, J. Adam *et al.*, “Determination of the event collision time with the ALICE detector at the LHC”, *Eur. Phys. J. Plus* **132** (2017) 99, arXiv:1610.03055 [physics.ins-det].
- [16] ALICE Collaboration, E. Abbas *et al.*, “Performance of the ALICE VZERO system”, *JINST* **8** (2013) P10016, arXiv:1306.3130 [nucl-ex].
- [17] ALICE Collaboration, B. Abelev *et al.*, “Centrality determination of Pb – Pb collisions at $\sqrt{s_{\text{NN}}} = 2.76$ TeV with ALICE”, *Phys. Rev. C* **88** (2013) 044909, arXiv:1301.4361 [nucl-ex].
- [18] ALICE Collaboration, S. Acharya *et al.*, “Centrality determination in heavy ion collisions”, ALICE-PUBLIC-2018-011 (2018). <https://cds.cern.ch/record/2636623>.
- [19] ALICE Collaboration, S. Acharya *et al.*, “ J/ψ elliptic and triangular flow in Pb – Pb collisions at $\sqrt{s_{\text{NN}}} = 5.02$ TeV”, *JHEP* **10** (2020) 141, arXiv:2005.14518 [nucl-ex].
- [20] ALICE Collaboration, K. Aamodt *et al.*, “Strange particle production in proton-proton collisions at $\sqrt{s} = 0.9$ TeV with ALICE at the LHC”, *Eur. Phys. J. C* **71** (2011) 1594, arXiv:1012.3257 [hep-ex].
- [21] ALICE Collaboration, B. Abelev *et al.*, “ K_S^0 and Λ production in Pb – Pb collisions at $\sqrt{s_{\text{NN}}} = 2.76$ TeV”, *Phys. Rev. Lett.* **111** (2013) 222301, arXiv:1307.5530 [nucl-ex].

- [22] **ALICE** Collaboration, S. Acharya *et al.*, “Multiplicity dependence of (multi-)strange hadron production in proton-proton collisions at $\sqrt{s} = 13$ TeV”, *Eur. Phys. J. C* **80** (2020) 167, arXiv:1908.01861 [nucl-ex].
- [23] **ALICE** Collaboration, J. Adam *et al.*, “Enhanced production of multi-strange hadrons in high-multiplicity proton-proton collisions”, *Nature Phys.* **13** (2017) 535–539, arXiv:1606.07424 [nucl-ex].
- [24] X.-N. Wang and M. Gyulassy, “HIJING: A monte carlo model for multiple jet production in pp, pA, and AA collisions”, *Phys. Rev. D* **44** (1991) 3501–3516.
- [25] R. Brunand *et al.*, “GEANT Detector Description and Simulation Tool, Program Library Long Write-up”,. <https://doi.org/10.17181/CERN.MUHF.DMJ1>.
- [26] **ALICE** Collaboration, B. Abelev *et al.*, “Multi-strange baryon production at mid-rapidity in Pb – Pb collisions at $\sqrt{s_{NN}} = 2.76$ TeV”, *Phys. Lett. B* **728** (2014) 216–227, arXiv:1307.5543 [nucl-ex]. [Erratum: *Phys.Lett.B* 734, 409–410 (2014)].
- [27] **ALICE** Collaboration, S. Acharya *et al.*, “Production of charged pions, kaons, and (anti-)protons in Pb – Pb and inelastic *pp* collisions at $\sqrt{s_{NN}} = 5.02$ TeV”, *Phys. Rev. C* **101** (2020) 044907, arXiv:1910.07678 [nucl-ex].
- [28] **ALICE** Collaboration, B. Abelev *et al.*, “Centrality dependence of π , *k*, and *p* production in Pb – Pb collisions at $\sqrt{s_{NN}} = 2.76$ TeV”, *Phys. Rev. C* **88** (2013) 044910, arXiv:1303.0737 [hep-ex].
- [29] S. Agostinelli *et al.*, “GEANT4 – a simulation toolkit”, *Nucl. Instrum. Meth. A* **506** (2003) 250–303.
- [30] **STAR** Collaboration, B. I. Abelev *et al.*, “Observation of an Antimatter Hypernucleus”, *Science* **328** (2010) 58–62, arXiv:1003.2030 [nucl-ex].

K. Gwizdziel ¹³³, L. Gyulai ¹³⁶, M.K. Habib ⁹⁷, C. Hadjidakis ⁷², F.U. Haider ⁹¹, H. Hamagaki ⁷⁶,
 A. Hamdi ⁷⁴, M. Hamid ⁶, Y. Han ¹³⁸, R. Hannigan ¹⁰⁸, M.R. Haque ¹³³, J.W. Harris ¹³⁷, A. Harton ⁹,
 H. Hassan ⁸⁷, D. Hatzifotiadou ⁵⁰, P. Hauer ⁴², L.B. Havener ¹³⁷, S.T. Heckel ⁹⁵, E. Hellbär ⁹⁷,
 H. Helstrup ³⁴, M. Hemmer ⁶³, T. Herman ³⁵, G. Herrera Corral ⁸, F. Herrmann ¹³⁵, S. Herrmann ¹²⁶,
 K.F. Hetland ³⁴, B. Heybeck ⁶³, H. Hillemanns ³², B. Hippolyte ¹²⁷, F.W. Hoffmann ⁶⁹, B. Hofman ⁵⁸,
 B. Hohlweger ⁸⁴, G.H. Hong ¹³⁸, M. Horst ⁹⁵, A. Horzyk ², Y. Hou ⁶, P. Hristov ³², C. Hughes ¹²⁰,
 P. Huhn ⁶³, L.M. Huhta ¹¹⁵, C.V. Hulse ⁷², T.J. Humanic ⁸⁸, A. Hutson ¹¹⁴, D. Hutter ³⁸, J.P. Iddon ¹¹⁷,
 R. Ilkaev ¹⁴⁰, H. Ilyas ¹³, M. Inaba ¹²³, G.M. Innocenti ³², M. Ippolitov ¹⁴⁰, A. Isakov ⁸⁶, T. Isidori ¹¹⁶,
 M.S. Islam ⁹⁹, M. Ivanov ⁹⁷, M. Ivanov ¹², V. Ivanov ¹⁴⁰, M. Jablonski ², B. Jacak ⁷⁴, N. Jacazio ³²,
 P.M. Jacobs ⁷⁴, S. Jadlovská ¹⁰⁶, J. Jadlovsky ¹⁰⁶, S. Jaelani ⁸², L. Jaffe ³⁸, C. Jahnke ¹¹¹,
 M.J. Jakubowska ¹³³, M.A. Janik ¹³³, T. Janson ⁶⁹, M. Jercic ⁸⁹, S. Jia ¹⁰, A.A.P. Jimenez ⁶⁴, F. Jonas ⁸⁷,
 J.M. Jowett ^{32,97}, J. Jung ⁶³, M. Jung ⁶³, A. Junique ³², A. Jusko ¹⁰⁰, M.J. Kabus ^{32,133}, J. Kaewjai ¹⁰⁵,
 P. Kalinak ⁵⁹, A.S. Kalteyer ⁹⁷, A. Kalweit ³², V. Kaplin ¹⁴⁰, A. Karasu Uysal ⁷¹, D. Karatovic ⁸⁹,
 O. Karavichev ¹⁴⁰, T. Karavicheva ¹⁴⁰, P. Karczmarczyk ¹³³, E. Karpechev ¹⁴⁰, U. Kebschull ⁶⁹,
 R. Keidel ¹³⁹, D.L.D. Keijdener ⁵⁸, M. Keil ³², B. Ketzer ⁴², S.S. Khade ⁴⁷, A.M. Khan ⁶, S. Khan ¹⁵,
 A. Khanzadeev ¹⁴⁰, Y. Kharlov ¹⁴⁰, A. Khatun ^{116,15}, A. Khuntia ¹⁰⁷, M.B. Kidson ¹¹³, B. Kileng ³⁴,
 B. Kim ¹⁰⁴, C. Kim ¹⁶, D.J. Kim ¹¹⁵, E.J. Kim ⁶⁸, J. Kim ¹³⁸, J.S. Kim ⁴⁰, J. Kim ⁶⁸, M. Kim ^{18,94},
 S. Kim ¹⁷, T. Kim ¹³⁸, K. Kimura ⁹², S. Kirsch ⁶³, I. Kisel ³⁸, S. Kiselev ¹⁴⁰, A. Kisiel ¹³³,
 J.P. Kitowski ², J.L. Klay ⁵, J. Klein ³², S. Klein ⁷⁴, C. Klein-Bösing ¹³⁵, M. Kleiner ⁶³,
 T. Klemenz ⁹⁵, A. Kluge ³², A.G. Knospe ¹¹⁴, C. Kobdaj ¹⁰⁵, T. Kollegger ⁹⁷, A. Kondratyev ¹⁴¹,
 N. Kondratyeva ¹⁴⁰, E. Kondratyuk ¹⁴⁰, J. König ⁶³, S.A. Königstorfer ⁹⁵, P.J. Konopka ³²,
 G. Kornakov ¹³³, S.D. Koryciak ², A. Kotliarov ⁸⁶, V. Kovalenko ¹⁴⁰, M. Kowalski ¹⁰⁷,
 V. Kozuharov ³⁶, I. Králik ⁵⁹, A. Kravčáková ³⁷, L. Krcaľ ^{32,38}, L. Kreis ⁹⁷, M. Krivda ^{100,59},
 F. Krizek ⁸⁶, K. Krizkova Gajdosova ³², M. Kroesen ⁹⁴, M. Krüger ⁶³, D.M. Krupova ³⁵,
 E. Kryshen ¹⁴⁰, V. Kučera ³², C. Kuhn ¹²⁷, P.G. Kuijer ⁸⁴, T. Kumaoka ¹²³, D. Kumar ¹³², L. Kumar ⁹⁰,
 N. Kumar ⁹⁰, S. Kumar ³¹, S. Kundu ³², P. Kurashvili ⁷⁹, A. Kurepin ¹⁴⁰, A.B. Kurepin ¹⁴⁰,
 A. Kuryakin ¹⁴⁰, S. Kushpil ⁸⁶, J. Kvapil ¹⁰⁰, M.J. Kweon ⁵⁷, J.Y. Kwon ⁵⁷, Y. Kwon ¹³⁸, S.L. La
 Pointe ³⁸, P. La Rocca ²⁶, A. Lakrathok ¹⁰⁵, M. Lamanna ³², R. Langoy ¹¹⁹, P. Larionov ³², E. Laudi ³²,
 L. Lautner ^{32,95}, R. Lavicka ¹⁰², T. Lazareva ¹⁴⁰, R. Lea ^{131,54}, H. Lee ¹⁰⁴, G. Legras ¹³⁵,
 J. Lehrbach ³⁸, T.M. Lelek ², R.C. Lemmon ⁸⁵, I. León Monzón ¹⁰⁹, M.M. Lesch ⁹⁵, E.D. Lesser ¹⁸,
 P. Lévai ¹³⁶, X. Li ¹⁰, X.L. Li ⁶, J. Lien ¹¹⁹, R. Lietava ¹⁰⁰, I. Likmeta ¹¹⁴, B. Lim ²⁴, S.H. Lim ¹⁶,
 V. Lindenstruth ³⁸, A. Lindner ⁴⁵, C. Lippmann ⁹⁷, A. Liu ¹⁸, D.H. Liu ⁶, J. Liu ¹¹⁷, I.M. Lofnes ²⁰,
 C. Loizides ⁸⁷, S. Lokos ¹⁰⁷, J. Lomker ⁵⁸, P. Loncar ³³, J.A. Lopez ⁹⁴, X. Lopez ¹²⁵, E. López
 Torres ⁷, P. Lu ^{97,118}, J.R. Luhder ¹³⁵, M. Lunardon ²⁷, G. Luparello ⁵⁶, Y.G. Ma ³⁹, A. Maevskaya ¹⁴⁰,
 M. Mager ³², A. Maire ¹²⁷, M.V. Makariev ³⁶, M. Malaev ¹⁴⁰, G. Malfattore ²⁵, N.M. Malik ⁹¹,
 Q.W. Malik ¹⁹, S.K. Malik ⁹¹, L. Malinina ^{VI,141}, D. Mal'Kevich ¹⁴⁰, D. Mallick ⁸⁰, N. Mallick ⁴⁷,
 G. Mandaglio ^{30,52}, S.K. Mandal ⁷⁹, V. Manko ¹⁴⁰, F. Manso ¹²⁵, V. Manzari ⁴⁹, Y. Mao ⁶,
 G.V. Margagliotti ²³, A. Margotti ⁵⁰, A. Marín ⁹⁷, C. Markert ¹⁰⁸, P. Martinengo ³², J.L. Martinez ¹¹⁴,
 M.I. Martínez ⁴⁴, G. Martínez García ¹⁰³, S. Masciocchi ⁹⁷, M. Maserà ²⁴, A. Masoni ⁵¹,
 L. Massacrier ⁷², A. Mastroserio ^{129,49}, O. Matonoha ⁷⁵, P.F.T. Matuoka ¹¹⁰, A. Matyja ¹⁰⁷, C. Mayer ¹⁰⁷,
 A.L. Mazuecos ³², F. Mazzaschi ²⁴, M. Mazzilli ³², J.E. Mdhuli ¹²¹, A.F. Mechler ⁶³, Y. Melikyan ^{43,140},
 A. Menchaca-Rocha ⁶⁶, E. Meninno ^{102,28}, A.S. Menon ¹¹⁴, M. Meres ¹², S. Mhlanga ^{113,67}, Y. Miake ¹²³,
 L. Micheletti ⁵⁵, L.C. Migliorin ¹²⁶, D.L. Mihaylov ⁹⁵, K. Mikhaylov ^{141,140}, A.N. Mishra ¹³⁶,
 D. Miśkowiec ⁹⁷, A. Modak ⁴, A.P. Mohanty ⁵⁸, B. Mohanty ⁸⁰, M. Mohisin Khan ^{IV,15},
 M.A. Molander ⁴³, Z. Moravcova ⁸³, C. Mordasini ⁹⁵, D.A. Moreira De Godoy ¹³⁵, I. Morozov ¹⁴⁰,
 A. Morsch ³², T. Mrnjavac ³², V. Muccifora ⁴⁸, S. Muhuri ¹³², J.D. Mulligan ⁷⁴, A. Mulliri ²²,
 M.G. Munhoz ¹¹⁰, R.H. Munzer ⁶³, H. Murakami ¹²², S. Murray ¹¹³, L. Musa ³², J. Musinsky ⁵⁹,
 J.W. Myrcha ¹³³, B. Naik ¹²¹, A.I. Nambrath ¹⁸, B.K. Nandi ⁴⁶, R. Nania ⁵⁰, E. Nappi ⁴⁹,
 A.F. Nassirpour ^{17,75}, A. Nath ⁹⁴, C. Nattrass ¹²⁰, M.N. Naydenov ³⁶, A. Neagu ¹⁹, A. Negru ¹²⁴,
 L. Nellen ⁶⁴, S.V. Nesbo ³⁴, G. Neskovic ³⁸, D. Nesterov ¹⁴⁰, B.S. Nielsen ⁸³, E.G. Nielsen ⁸³,
 S. Nikolaev ¹⁴⁰, S. Nikulin ¹⁴⁰, V. Nikulin ¹⁴⁰, F. Noferini ⁵⁰, S. Noh ¹¹, P. Nomokonov ¹⁴¹,
 J. Norman ¹¹⁷, N. Novitzky ¹²³, P. Nowakowski ¹³³, A. Nyanin ¹⁴⁰, J. Nystrand ²⁰, M. Ogino ⁷⁶,
 A. Ohlson ⁷⁵, V.A. Okorokov ¹⁴⁰, J. Oleniacz ¹³³, A.C. Oliveira Da Silva ¹²⁰, M.H. Oliver ¹³⁷,
 A. Onnerstad ¹¹⁵, C. Oppedisano ⁵⁵, A. Ortiz Velasquez ⁶⁴, J. Otwinowski ¹⁰⁷, M. Oya ⁹², K. Oyama ⁷⁶,
 Y. Pachmayer ⁹⁴, S. Padhan ⁴⁶, D. Pagano ^{131,54}, G. Paić ⁶⁴, A. Palasciano ⁴⁹, S. Panebianco ¹²⁸,
 H. Park ¹²³, H. Park ¹⁰⁴, J. Park ⁵⁷, J.E. Parkkila ³², R.N. Patra ⁹¹, B. Paul ²², H. Pei ⁶,

T. Peitzmann⁵⁸, X. Peng⁶, M. Pennisi²⁴, L.G. Pereira⁶⁵, D. Peresunko¹⁴⁰, G.M. Perez⁷,
 S. Perrin¹²⁸, Y. Pestov¹⁴⁰, V. Petráček³⁵, V. Petrov¹⁴⁰, M. Petrovici⁴⁵, R.P. Pezzi^{103,65}, S. Piano⁵⁶,
 M. Pikna¹², P. Pillot¹⁰³, O. Pinazza^{50,32}, L. Pinsky¹¹⁴, C. Pinto⁹⁵, S. Pisano⁴⁸, M. Płoskoń⁷⁴,
 M. Planinic⁸⁹, F. Pliquett⁶³, M.G. Poghosyan⁸⁷, B. Polichtchouk¹⁴⁰, S. Politano²⁹, N. Poljak⁸⁹,
 A. Pop⁴⁵, S. Porteboeuf-Houssais¹²⁵, V. Pozdniakov¹⁴¹, I.Y. Pozos⁴⁴, K.K. Pradhan⁴⁷,
 S.K. Prasad⁴, S. Prasad⁴⁷, R. Preghenella⁵⁰, F. Prino⁵⁵, C.A. Pruneau¹³⁴, I. Pshenichnov¹⁴⁰,
 M. Puccio³², S. Pucillo²⁴, Z. Pugelova¹⁰⁶, S. Qiu⁸⁴, L. Quaglia²⁴, R.E. Quishpe¹¹⁴, S. Ragoni¹⁴,
 A. Rakotozafindrabe¹²⁸, L. Ramello^{130,55}, F. Rami¹²⁷, S.A.R. Ramirez⁴⁴, T.A. Rancien⁷³, M. Rasa²⁶,
 S.S. Räsänen⁴³, R. Rath⁵⁰, M.P. Rauch²⁰, I. Ravasenga⁸⁴, K.F. Read^{87,120}, C. Reckziegel¹¹²,
 A.R. Redelbach³⁸, K. Redlich^{7,79}, C.A. Reetz⁹⁷, A. Rehman²⁰, F. Reidt³², H.A. Reme-Ness³⁴,
 Z. Rescakova³⁷, K. Reygers⁹⁴, A. Riabov¹⁴⁰, V. Riabov¹⁴⁰, R. Ricci²⁸, M. Richter¹⁹,
 A.A. Riedel⁹⁵, W. Riegler³², C. Ristea⁶², M. Rodríguez Cahuantzi⁴⁴, K. Røed¹⁹, R. Rogalev¹⁴⁰,
 E. Rogochaya¹⁴¹, T.S. Rogoschinski⁶³, D. Rohr³², D. Röhrich²⁰, P.F. Rojas⁴⁴, S. Rojas Torres³⁵,
 P.S. Rokita¹³³, G. Romanenko¹⁴¹, F. Ronchetti⁴⁸, A. Rosano^{30,52}, E.D. Rosas⁶⁴, K. Roslon¹³³,
 A. Rossi⁵³, A. Roy⁴⁷, S. Roy⁴⁶, N. Rubini²⁵, O.V. Rueda¹¹⁴, D. Ruggiano¹³³, R. Rui²³,
 B. Rumyantsev¹⁴¹, P.G. Russek², R. Russo⁸⁴, A. Rustamov⁸¹, E. Ryabinkin¹⁴⁰, Y. Ryabov¹⁴⁰,
 A. Rybicki¹⁰⁷, H. Rytkonen¹¹⁵, W. Rzeska¹³³, O.A.M. Saarimaki⁴³, R. Sadek¹⁰³, S. Sadhu³¹,
 S. Sadovsky¹⁴⁰, J. Saetre²⁰, K. Šafařík³⁵, S.K. Saha⁴, S. Saha⁸⁰, B. Sahoo⁴⁶, B. Sahoo⁴⁷,
 R. Sahoo⁴⁷, S. Sahoo⁶⁰, D. Sahu⁴⁷, P.K. Sahu⁶⁰, J. Saini¹³², K. Sajdakova³⁷, S. Sakai¹²³,
 M.P. Salvan⁹⁷, S. Sambyal⁹¹, I. Sanna^{32,95}, T.B. Saramela¹¹⁰, D. Sarkar¹³⁴, N. Sarkar¹³², P. Sarma⁴¹,
 V. Sarritzu²², V.M. Sarti⁹⁵, M.H.P. Sas¹³⁷, J. Schambach⁸⁷, H.S. Scheid⁶³, C. Schiaua⁴⁵,
 R. Schicker⁹⁴, A. Schmah⁹⁴, C. Schmidt⁹⁷, H.R. Schmidt⁹³, M.O. Schmidt³², M. Schmidt⁹³,
 N.V. Schmidt⁸⁷, A.R. Schmier¹²⁰, R. Schotter¹²⁷, A. Schröter³⁸, J. Schukraft³², K. Schwarz⁹⁷,
 K. Schweda⁹⁷, G. Scioli²⁵, E. Scomparin⁵⁵, J.E. Seger¹⁴, Y. Sekiguchi¹²², D. Sekihata¹²²,
 I. Selyuzhenkov^{97,140}, S. Senyukov¹²⁷, J.J. Seo⁵⁷, D. Serebryakov¹⁴⁰, L. Šerkšnytė⁹⁵,
 A. Sevcenco⁶², T.J. Shaba⁶⁷, A. Shabetai¹⁰³, R. Shahoyan³², A. Shangaraev¹⁴⁰, A. Sharma⁹⁰,
 B. Sharma⁹¹, D. Sharma⁴⁶, H. Sharma¹⁰⁷, M. Sharma⁹¹, S. Sharma⁷⁶, S. Sharma⁹¹,
 U. Sharma⁹¹, A. Shatat⁷², O. Sheibani¹¹⁴, K. Shigaki⁹², M. Shimomura⁷⁷, J. Shin¹¹, S. Shirinkin¹⁴⁰,
 Q. Shou³⁹, Y. Sibiriak¹⁴⁰, S. Siddhanta⁵¹, T. Siemiarczuk⁷⁹, T.F. Silva¹¹⁰, D. Silvermyr⁷⁵,
 T. Simantathammakul¹⁰⁵, R. Simeonov³⁶, B. Singh⁹¹, B. Singh⁹⁵, R. Singh⁸⁰, R. Singh⁹¹, R. Singh⁴⁷,
 S. Singh¹⁵, V.K. Singh¹³², V. Singhal¹³², T. Sinha⁹⁹, B. Sitar¹², M. Sitta^{130,55}, T.B. Skaali¹⁹,
 G. Skorodumovs⁹⁴, M. Słupecki⁴³, N. Smirnov¹³⁷, R.J.M. Snellings⁵⁸, E.H. Solheim¹⁹, J. Song¹¹⁴,
 A. Songmoolnak¹⁰⁵, F. Soramel²⁷, A.B. Soto-herandez⁸⁸, R. Spijkers⁸⁴, I. Sputowska¹⁰⁷, J. Staa⁷⁵,
 J. Stachel⁹⁴, I. Stan⁶², P.J. Steffanic¹²⁰, S.F. Stiefelmaier⁹⁴, D. Stocco¹⁰³, I. Storehaug¹⁹,
 P. Stratmann¹³⁵, S. Strazzi²⁵, C.P. Stylianidis⁸⁴, A.A.P. Suaide¹¹⁰, C. Suire⁷², M. Sukhanov¹⁴⁰,
 M. Suljic³², R. Sultanov¹⁴⁰, V. Sumberia⁹¹, S. Sumowidagdo⁸², S. Swain⁶⁰, I. Szarka¹²,
 M. Szymkowski¹³³, S.F. Taghavi⁹⁵, G. Taillepied⁹⁷, J. Takahashi¹¹¹, G.J. Tambave²⁰, S. Tang^{125,6},
 Z. Tang¹¹⁸, J.D. Tapia Takaki¹¹⁶, N. Tapus¹²⁴, L.A. Tarasovicova¹³⁵, M.G. Tazila⁴⁵, G.F. Tassielli³¹,
 A. Tauro³², G. Tejeda Muñoz⁴⁴, A. Telesca³², L. Terlizzi²⁴, C. Terrevoli¹¹⁴, S. Thakur⁴,
 D. Thomas¹⁰⁸, A. Tikhonov¹⁴⁰, A.R. Timmins¹¹⁴, M. Tkacik¹⁰⁶, T. Tkacik¹⁰⁶, A. Toia⁶³,
 R. Tokumoto⁹², N. Topilskaya¹⁴⁰, M. Toppi⁴⁸, F. Torres-Acosta¹⁸, T. Tork⁷², A.G. Torres Ramos³¹,
 A. Trifiró^{30,52}, A.S. Triolo^{32,30,52}, S. Tripathy⁵⁰, T. Tripathy⁴⁶, S. Trogolo³², V. Trubnikov³,
 W.H. Trzaska¹¹⁵, T.P. Trzcinski¹³³, A. Tumkin¹⁴⁰, R. Turrisi⁵³, T.S. Tveter¹⁹, K. Ullaland²⁰,
 B. Ulukutlu⁹⁵, A. Uras¹²⁶, M. Urioni^{54,131}, G.L. Usai²², M. Vala³⁷, N. Valle²¹, L.V.R. van
 Doremalen⁵⁸, M. van Leeuwen⁸⁴, C.A. van Veen⁹⁴, R.J.G. van Weelden⁸⁴, P. Vande Vyvre³²,
 D. Varga¹³⁶, Z. Varga¹³⁶, M. Vasileiou⁷⁸, A. Vasiliev¹⁴⁰, O. Vázquez Doce⁴⁸, V. Vechernin¹⁴⁰,
 E. Vercellin²⁴, S. Vergara Limón⁴⁴, L. Vermunt⁹⁷, R. Vértesi¹³⁶, M. Verweij⁵⁸, L. Vickovic³³,
 Z. Vilakazi¹²¹, O. Villalobos Baillie¹⁰⁰, A. Villani²³, G. Vino⁴⁹, A. Vinogradov¹⁴⁰, T. Virgili²⁸,
 M.M.O. Virta¹¹⁵, V. Vislavicius⁷⁵, A. Vodopyanov¹⁴¹, B. Volkel³², M.A. Völkl⁹⁴, K. Voloshin¹⁴⁰,
 S.A. Voloshin¹³⁴, G. Volpe³¹, B. von Haller³², I. Vorobyev⁹⁵, N. Vozniuk¹⁴⁰, J. Vrláková³⁷,
 C. Wang³⁹, D. Wang³⁹, Y. Wang³⁹, A. Wegrzynek³², F.T. Weiglhofer³⁸, S.C. Wenzel³²,
 J.P. Wessels¹³⁵, S.L. Weyhmler¹³⁷, J. Wiechula⁶³, J. Wikne¹⁹, G. Wilk⁷⁹, J. Wilkinson⁹⁷,
 G.A. Willems¹³⁵, B. Windelband⁹⁴, M. Winn¹²⁸, J.R. Wright¹⁰⁸, W. Wu³⁹, Y. Wu¹¹⁸, R. Xu⁶,
 A. Yadav⁴², A.K. Yadav¹³², S. Yalcin⁷¹, Y. Yamaguchi⁹², S. Yang²⁰, S. Yano⁹², Z. Yin⁶,
 I.-K. Yoo¹⁶, J.H. Yoon⁵⁷, S. Yuan²⁰, A. Yuncu⁹⁴, V. Zaccolo²³, C. Zampolli³², F. Zanone⁹⁴,
 N. Zardoshti³², A. Zarochentsev¹⁴⁰, P. Závada⁶¹, N. Zaviyalov¹⁴⁰, M. Zhalov¹⁴⁰, B. Zhang⁶,

L. Zhang ³⁹, S. Zhang ³⁹, X. Zhang ⁶, Y. Zhang¹¹⁸, Z. Zhang ⁶, M. Zhao ¹⁰, V. Zhrebchevskii ¹⁴⁰,
Y. Zhi¹⁰, D. Zhou ⁶, Y. Zhou ⁸³, J. Zhu ^{97,6}, Y. Zhu⁶, S.C. Zugravel ⁵⁵, N. Zurlo ^{131,54}

Affiliation Notes

^I Deceased

^{II} Also at: Max-Planck-Institut für Physik, Munich, Germany

^{III} Also at: Italian National Agency for New Technologies, Energy and Sustainable Economic Development (ENEA), Bologna, Italy

^{IV} Also at: Department of Applied Physics, Aligarh Muslim University, Aligarh, India

^V Also at: Institute of Theoretical Physics, University of Wrocław, Poland

^{VI} Also at: An institution covered by a cooperation agreement with CERN

Collaboration Institutes

¹ A.I. Alikhanyan National Science Laboratory (Yerevan Physics Institute) Foundation, Yerevan, Armenia

² AGH University of Science and Technology, Cracow, Poland

³ Bogolyubov Institute for Theoretical Physics, National Academy of Sciences of Ukraine, Kiev, Ukraine

⁴ Bose Institute, Department of Physics and Centre for Astroparticle Physics and Space Science (CAPSS), Kolkata, India

⁵ California Polytechnic State University, San Luis Obispo, California, United States

⁶ Central China Normal University, Wuhan, China

⁷ Centro de Aplicaciones Tecnológicas y Desarrollo Nuclear (CEADEN), Havana, Cuba

⁸ Centro de Investigación y de Estudios Avanzados (CINVESTAV), Mexico City and Mérida, Mexico

⁹ Chicago State University, Chicago, Illinois, United States

¹⁰ China Institute of Atomic Energy, Beijing, China

¹¹ Chungbuk National University, Cheongju, Republic of Korea

¹² Comenius University Bratislava, Faculty of Mathematics, Physics and Informatics, Bratislava, Slovak Republic

¹³ COMSATS University Islamabad, Islamabad, Pakistan

¹⁴ Creighton University, Omaha, Nebraska, United States

¹⁵ Department of Physics, Aligarh Muslim University, Aligarh, India

¹⁶ Department of Physics, Pusan National University, Pusan, Republic of Korea

¹⁷ Department of Physics, Sejong University, Seoul, Republic of Korea

¹⁸ Department of Physics, University of California, Berkeley, California, United States

¹⁹ Department of Physics, University of Oslo, Oslo, Norway

²⁰ Department of Physics and Technology, University of Bergen, Bergen, Norway

²¹ Dipartimento di Fisica, Università di Pavia, Pavia, Italy

²² Dipartimento di Fisica dell'Università and Sezione INFN, Cagliari, Italy

²³ Dipartimento di Fisica dell'Università and Sezione INFN, Trieste, Italy

²⁴ Dipartimento di Fisica dell'Università and Sezione INFN, Turin, Italy

²⁵ Dipartimento di Fisica e Astronomia dell'Università and Sezione INFN, Bologna, Italy

²⁶ Dipartimento di Fisica e Astronomia dell'Università and Sezione INFN, Catania, Italy

²⁷ Dipartimento di Fisica e Astronomia dell'Università and Sezione INFN, Padova, Italy

²⁸ Dipartimento di Fisica 'E.R. Caianiello' dell'Università and Gruppo Collegato INFN, Salerno, Italy

²⁹ Dipartimento DISAT del Politecnico and Sezione INFN, Turin, Italy

³⁰ Dipartimento di Scienze MIFT, Università di Messina, Messina, Italy

³¹ Dipartimento Interateneo di Fisica 'M. Merlin' and Sezione INFN, Bari, Italy

³² European Organization for Nuclear Research (CERN), Geneva, Switzerland

³³ Faculty of Electrical Engineering, Mechanical Engineering and Naval Architecture, University of Split, Split, Croatia

³⁴ Faculty of Engineering and Science, Western Norway University of Applied Sciences, Bergen, Norway

³⁵ Faculty of Nuclear Sciences and Physical Engineering, Czech Technical University in Prague, Prague, Czech Republic

³⁶ Faculty of Physics, Sofia University, Sofia, Bulgaria

³⁷ Faculty of Science, P.J. Šafárik University, Košice, Slovak Republic

³⁸ Frankfurt Institute for Advanced Studies, Johann Wolfgang Goethe-Universität Frankfurt, Frankfurt, Germany

- ³⁹ Fudan University, Shanghai, China
⁴⁰ Gangneung-Wonju National University, Gangneung, Republic of Korea
⁴¹ Gauhati University, Department of Physics, Guwahati, India
⁴² Helmholtz-Institut für Strahlen- und Kernphysik, Rheinische Friedrich-Wilhelms-Universität Bonn, Bonn, Germany
⁴³ Helsinki Institute of Physics (HIP), Helsinki, Finland
⁴⁴ High Energy Physics Group, Universidad Autónoma de Puebla, Puebla, Mexico
⁴⁵ Horia Hulubei National Institute of Physics and Nuclear Engineering, Bucharest, Romania
⁴⁶ Indian Institute of Technology Bombay (IIT), Mumbai, India
⁴⁷ Indian Institute of Technology Indore, Indore, India
⁴⁸ INFN, Laboratori Nazionali di Frascati, Frascati, Italy
⁴⁹ INFN, Sezione di Bari, Bari, Italy
⁵⁰ INFN, Sezione di Bologna, Bologna, Italy
⁵¹ INFN, Sezione di Cagliari, Cagliari, Italy
⁵² INFN, Sezione di Catania, Catania, Italy
⁵³ INFN, Sezione di Padova, Padova, Italy
⁵⁴ INFN, Sezione di Pavia, Pavia, Italy
⁵⁵ INFN, Sezione di Torino, Turin, Italy
⁵⁶ INFN, Sezione di Trieste, Trieste, Italy
⁵⁷ Inha University, Incheon, Republic of Korea
⁵⁸ Institute for Gravitational and Subatomic Physics (GRASP), Utrecht University/Nikhef, Utrecht, Netherlands
⁵⁹ Institute of Experimental Physics, Slovak Academy of Sciences, Košice, Slovak Republic
⁶⁰ Institute of Physics, Homi Bhabha National Institute, Bhubaneswar, India
⁶¹ Institute of Physics of the Czech Academy of Sciences, Prague, Czech Republic
⁶² Institute of Space Science (ISS), Bucharest, Romania
⁶³ Institut für Kernphysik, Johann Wolfgang Goethe-Universität Frankfurt, Frankfurt, Germany
⁶⁴ Instituto de Ciencias Nucleares, Universidad Nacional Autónoma de México, Mexico City, Mexico
⁶⁵ Instituto de Física, Universidade Federal do Rio Grande do Sul (UFRGS), Porto Alegre, Brazil
⁶⁶ Instituto de Física, Universidad Nacional Autónoma de México, Mexico City, Mexico
⁶⁷ iThemba LABS, National Research Foundation, Somerset West, South Africa
⁶⁸ Jeonbuk National University, Jeonju, Republic of Korea
⁶⁹ Johann-Wolfgang-Goethe Universität Frankfurt Institut für Informatik, Fachbereich Informatik und Mathematik, Frankfurt, Germany
⁷⁰ Korea Institute of Science and Technology Information, Daejeon, Republic of Korea
⁷¹ KTO Karatay University, Konya, Turkey
⁷² Laboratoire de Physique des 2 Infinis, Irène Joliot-Curie, Orsay, France
⁷³ Laboratoire de Physique Subatomique et de Cosmologie, Université Grenoble-Alpes, CNRS-IN2P3, Grenoble, France
⁷⁴ Lawrence Berkeley National Laboratory, Berkeley, California, United States
⁷⁵ Lund University Department of Physics, Division of Particle Physics, Lund, Sweden
⁷⁶ Nagasaki Institute of Applied Science, Nagasaki, Japan
⁷⁷ Nara Women's University (NWU), Nara, Japan
⁷⁸ National and Kapodistrian University of Athens, School of Science, Department of Physics, Athens, Greece
⁷⁹ National Centre for Nuclear Research, Warsaw, Poland
⁸⁰ National Institute of Science Education and Research, Homi Bhabha National Institute, Jatni, India
⁸¹ National Nuclear Research Center, Baku, Azerbaijan
⁸² National Research and Innovation Agency - BRIN, Jakarta, Indonesia
⁸³ Niels Bohr Institute, University of Copenhagen, Copenhagen, Denmark
⁸⁴ Nikhef, National institute for subatomic physics, Amsterdam, Netherlands
⁸⁵ Nuclear Physics Group, STFC Daresbury Laboratory, Daresbury, United Kingdom
⁸⁶ Nuclear Physics Institute of the Czech Academy of Sciences, Husinec-Řež, Czech Republic
⁸⁷ Oak Ridge National Laboratory, Oak Ridge, Tennessee, United States
⁸⁸ Ohio State University, Columbus, Ohio, United States
⁸⁹ Physics department, Faculty of science, University of Zagreb, Zagreb, Croatia
⁹⁰ Physics Department, Panjab University, Chandigarh, India
⁹¹ Physics Department, University of Jammu, Jammu, India

- ⁹² Physics Program and International Institute for Sustainability with Knotted Chiral Meta Matter (SKCM2), Hiroshima University, Hiroshima, Japan
- ⁹³ Physikalisches Institut, Eberhard-Karls-Universität Tübingen, Tübingen, Germany
- ⁹⁴ Physikalisches Institut, Ruprecht-Karls-Universität Heidelberg, Heidelberg, Germany
- ⁹⁵ Physik Department, Technische Universität München, Munich, Germany
- ⁹⁶ Politecnico di Bari and Sezione INFN, Bari, Italy
- ⁹⁷ Research Division and ExtreMe Matter Institute EMMI, GSI Helmholtzzentrum für Schwerionenforschung GmbH, Darmstadt, Germany
- ⁹⁸ Saga University, Saga, Japan
- ⁹⁹ Saha Institute of Nuclear Physics, Homi Bhabha National Institute, Kolkata, India
- ¹⁰⁰ School of Physics and Astronomy, University of Birmingham, Birmingham, United Kingdom
- ¹⁰¹ Sección Física, Departamento de Ciencias, Pontificia Universidad Católica del Perú, Lima, Peru
- ¹⁰² Stefan Meyer Institut für Subatomare Physik (SMI), Vienna, Austria
- ¹⁰³ SUBATECH, IMT Atlantique, Nantes Université, CNRS-IN2P3, Nantes, France
- ¹⁰⁴ Sungkyunkwan University, Suwon City, Republic of Korea
- ¹⁰⁵ Suranaree University of Technology, Nakhon Ratchasima, Thailand
- ¹⁰⁶ Technical University of Košice, Košice, Slovak Republic
- ¹⁰⁷ The Henryk Niewodniczanski Institute of Nuclear Physics, Polish Academy of Sciences, Cracow, Poland
- ¹⁰⁸ The University of Texas at Austin, Austin, Texas, United States
- ¹⁰⁹ Universidad Autónoma de Sinaloa, Culiacán, Mexico
- ¹¹⁰ Universidade de São Paulo (USP), São Paulo, Brazil
- ¹¹¹ Universidade Estadual de Campinas (UNICAMP), Campinas, Brazil
- ¹¹² Universidade Federal do ABC, Santo Andre, Brazil
- ¹¹³ University of Cape Town, Cape Town, South Africa
- ¹¹⁴ University of Houston, Houston, Texas, United States
- ¹¹⁵ University of Jyväskylä, Jyväskylä, Finland
- ¹¹⁶ University of Kansas, Lawrence, Kansas, United States
- ¹¹⁷ University of Liverpool, Liverpool, United Kingdom
- ¹¹⁸ University of Science and Technology of China, Hefei, China
- ¹¹⁹ University of South-Eastern Norway, Kongsberg, Norway
- ¹²⁰ University of Tennessee, Knoxville, Tennessee, United States
- ¹²¹ University of the Witwatersrand, Johannesburg, South Africa
- ¹²² University of Tokyo, Tokyo, Japan
- ¹²³ University of Tsukuba, Tsukuba, Japan
- ¹²⁴ University Politehnica of Bucharest, Bucharest, Romania
- ¹²⁵ Université Clermont Auvergne, CNRS/IN2P3, LPC, Clermont-Ferrand, France
- ¹²⁶ Université de Lyon, CNRS/IN2P3, Institut de Physique des 2 Infinis de Lyon, Lyon, France
- ¹²⁷ Université de Strasbourg, CNRS, IPHC UMR 7178, F-67000 Strasbourg, France, Strasbourg, France
- ¹²⁸ Université Paris-Saclay Centre d'Etudes de Saclay (CEA), IRFU, Département de Physique Nucléaire (DPhN), Saclay, France
- ¹²⁹ Università degli Studi di Foggia, Foggia, Italy
- ¹³⁰ Università del Piemonte Orientale, Vercelli, Italy
- ¹³¹ Università di Brescia, Brescia, Italy
- ¹³² Variable Energy Cyclotron Centre, Homi Bhabha National Institute, Kolkata, India
- ¹³³ Warsaw University of Technology, Warsaw, Poland
- ¹³⁴ Wayne State University, Detroit, Michigan, United States
- ¹³⁵ Westfälische Wilhelms-Universität Münster, Institut für Kernphysik, Münster, Germany
- ¹³⁶ Wigner Research Centre for Physics, Budapest, Hungary
- ¹³⁷ Yale University, New Haven, Connecticut, United States
- ¹³⁸ Yonsei University, Seoul, Republic of Korea
- ¹³⁹ Zentrum für Technologie und Transfer (ZTT), Worms, Germany
- ¹⁴⁰ Affiliated with an institute covered by a cooperation agreement with CERN
- ¹⁴¹ Affiliated with an international laboratory covered by a cooperation agreement with CERN.